Progress In Electromagnetics Research M, Vol. 110, 211–221, 2022

Torque Compensation Method of Switched Reluctance Motor Adopting MPC Based on TSF-DITC

Yang Yang[1], Aide Xu[2, *], Bing Leng[1], Jinghao Sun[1], and Kuo Li[2]

Abstract—Aiming at the problem of large torque ripple caused by large tracking error between actual torque and reference torque in commutation region in direct instantaneous torque control (DITC) algorithm of switched reluctance motor (SRM) based on torque sharing function (TSF), a torque compensation method combining TSF-DITC and model predictive control (MPC) is proposed. Sectors are subdivided in the commutation region according to the rotor position. Different voltage states are selected in different sectors to fully compensate for the tracking error between the actual phase torque and the reference torque distributed by TSF, and then the total torque ripple is greatly reduced. At the same time, the algorithm also effectively reduces the candidate voltage states at the current time and reduces the computational burden. The simulation comparison with TSF-DITC shows that the algorithm (TSF-PDITC) has better steady state and dynamic performance.

1. INTRODUCTION

Switched reluctance motor (SRM) has the characteristics of simple structure, strong robustness and strong fault tolerance, and is widely used in various electric drive and industrial fields [1–3]. However, due to the unique doubly salient structure of SRM and the highly nonlinear characteristics of the magnetic circuit, it also causes the problem of excessive torque ripple of SRM, which limits the further application of SRM.

Direct instantaneous torque control (DITC) based on torque sharing function (TSF) also known as TSF-DITC is currently one of the main methods to suppress the torque ripple of SRM. This method uses TSF to distribute the total torque to individual phase, and then the phase torque hysteresis drives the motor according to appropriate control rules. Reference [4] selects a multi-level converter on the basis of TSF-DITC and selects corresponding control rules in different conduction regions, which can accelerate the excitation and demagnetization of the commutation region and achieve fast torque tracking. Reference [5] proposes a direct instantaneous torque control method for SRM based on the optimal angle adaptive TSF. Reference [6] uses the dynamic shapeless TSF to improve the system efficiency in SRM torque control. Different commutation points have a great influence on the system performance. In short, although the TSF-DITC algorithm is simple, easy to implement and has a certain degree of torque ripple suppression effect, it is necessary to formulate complex hysteresis control rules in the commutation region, and it is difficult to optimize multiple performance indexes at the same time.

Model Predictive Control (MPC) is a novel multi-objective optimal control scheme for nonlinear systems, which uses a predictive model to calculate the value of the motor at the next sampling time [7–9]. Reference [10] uses the cost function of MPC to accurately track the reference flux linkage and combines the six basic voltage vectors in the classical DTC to reduce the torque ripple. A model

Received 8 April 2022, Accepted 23 May 2022, Scheduled 6 June 2022

* Corresponding author: Aide Xu (aidexu@dlmu.edu.cn).

[1] College of Electrical Engineering of Ships, Dalian Maritime University, Dalian 116026, China. [2] College of Information and Science Technology, Dalian Maritime University, Dalian 116026, China.

predictive current control is addressed in [11], which enhances the phase current tracking capability. In summary, MPC can replace traditional hysteretic control while avoiding complex commutation rules.

Based on this, this paper proposes a torque compensation method using TSF to distribute the torque of each phase and to adopt MPC for SRM. Firstly, the static electromagnetic characteristics of SRM are measured through the locked-rotor experiment, and the discrete prediction model of SRM is established. Secondly, according to the tracking error between the reference torque and the actual torque in the commutation region, a switching vector subregional selection rule is formulated for torque compensation, which not only reduces the torque ripple but also reduces the amount of calculation. In addition, a cost function containing a variable of torque is introduced to evaluate the prediction results, and the switching vector that minimizes the cost function is selected as the optimal switching vector to output to the motor. The simulation results show that the performance of the proposed predictive direct instantaneous torque control based on torque sharing function (TSF-PDITC) algorithm is better than the traditional TSF-DITC.

2. SRM MODEL

2.1. Mathematical Equation

The mathematical model of SRM is as follows:

$$\begin{cases} \dfrac{\mathrm{d}\psi_p}{\mathrm{d}t} = v_p - Ri_p, & p = 1,2,3 \\ \dfrac{\mathrm{d}\omega}{\mathrm{d}t} = \dfrac{1}{J}(T_e - T_L - D\omega), & T_e = \displaystyle\sum_{p=1}^{3} T_p \\ \dfrac{\mathrm{d}\theta}{\mathrm{d}t} = \omega \end{cases} \tag{1}$$

where ψ_p, v_p, and i_p correspond to the flux-linkage, voltage, and current of single phase. R is the SRM winding resistance, and θ is the rotor position. J, D, and ω are the moment of inertia, viscous friction, and motor speed, respectively. T_e, T_L, and T_p correspond to the total torque, load torque, and phase torque, respectively.

The instantaneous torque equation can be indicated as:

$$T_p = \left.\frac{\mathrm{d}W_c(\theta_p, i_p)}{\mathrm{d}\theta_p}\right|_{i_p=\text{const}} = \left.\frac{\mathrm{d}W_s(\theta_p, i_p)}{\mathrm{d}\theta_p}\right|_{\psi_p=\text{const}} \tag{2}$$

where $W_c = \int_0^i \psi(\theta, i)\mathrm{d}i$ is the co-energy, and $W_s = \int_0^\psi i(\theta, \psi)\mathrm{d}\psi$ is the stored field energy of phase winding.

2.2. Establishment of Flux-Linkage and Torque Model

Establishing an accurate nonlinear model for SRM is an important prerequisite for realizing high-performance torque control. This paper adopts the nonlinear flux-linkage and torque model proposed by Le-Huy in [12]. It is worth mentioning that this model only needs to measure the two flux-linkage characteristic curves of the aligned and unaligned positions through the locked-rotor experiment, and then the complete flux-linkage and torque characteristic curves can be obtained through the interpolation function. Figure 1 shows the locked-rotor experimental platform, and Figure 2(a) is the obtained flux-linkage characteristic curve. Figure 2(b) gives a schematic illustration of this method.

The expression of this model is shown by Equations (3) and (4):

$$\begin{cases} \psi = L_q i + \left[L_{dsat} i + A(1 - e^{-Bi}) - L_q i\right] f(\theta) \\ T = \left[\dfrac{(L_{dsat} - L_q)i^2}{2} + Ai - \dfrac{A(1 - e^{-Bi})}{B}\right] \frac{\mathrm{d}f(\theta)}{\mathrm{d}t} \end{cases} \tag{3}$$

$$\begin{cases} A = \psi_m - L_{dsat} I_m \\ B = (L_d - L_{dsat})/(\psi_m - L_{dsat} I_m) \\ f(\theta) = (2N_r^3/\pi^3)\theta^3 - (3N_r^2/\pi^2)\theta^2 + 1 \end{cases} \tag{4}$$

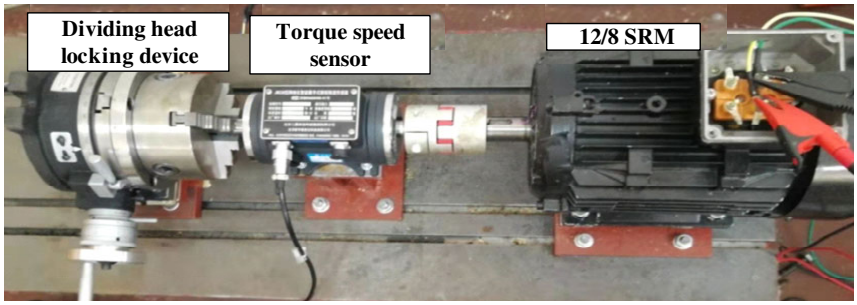

Figure 1. Locked rotor test platform of SRM.

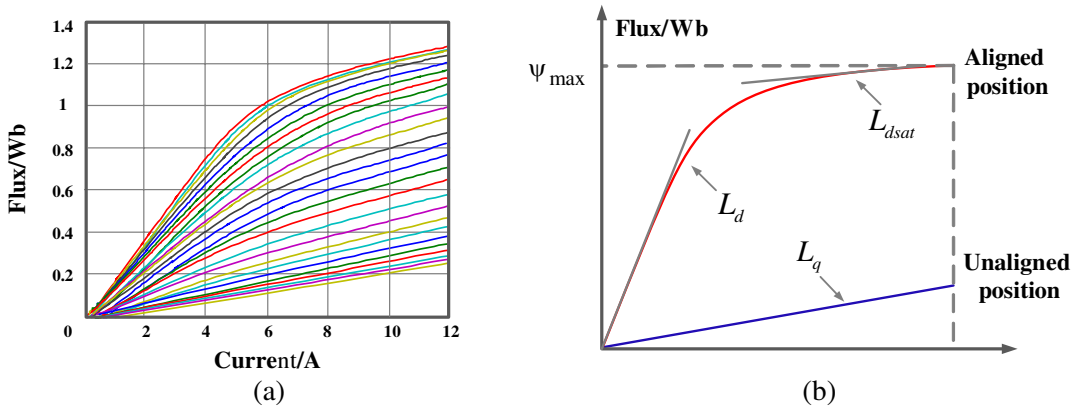

Figure 2. SRM (a) flux-linkage characteristics, (b) nonlinear mathematical model.

where L_d and L_q represent the motor inductance of center line of stator and rotor which are completely aligned and unaligned, respectively. L_{dsat} is the saturation inductance, ψ_m the maximum value of the flux-linkage, and I_m the maximum value of current corresponding to the ψ_m.

3. ANALYSIS OF TRADITIONAL TSF-DITC STRATEGY

3.1. TSF-DITC

Figure 3 shows the control diagram of TSF-DITC. The PI outputs the total reference torque T_e^*, and the TSF distributes the total reference torque to each phase to obtain the phase reference torque value, and then obtains the driving signal of each phase from the torque hysteresis, which is applied to the power converter to control the operation of the motor.

In this paper, the cosine TSF is selected. In one angular period of the rotor, the expression is as follows:

$$T_p^* = \begin{cases} 0, & (0 \le \theta_p \le \theta_{on}) \\ \dfrac{T_e^*}{2} - \dfrac{T_e^*}{2}\cos\dfrac{\pi}{\theta_{ov}}(\theta_p - \theta_{on}), & (\theta_{on} \le \theta_p \le \theta_{on} + \theta_{ov}) \\ T_e^*, & (\theta_{on} + \theta_{ov} \le \theta_p \le \theta_{off}) \\ \dfrac{T_e^*}{2} + \dfrac{T_e^*}{2}\cos\dfrac{\pi}{\theta_{ov}}(\theta_p - \theta_{off}), & (\theta_{off} \le \theta_p \le \theta_{off} + \theta_{ov}) \\ 0, & (\theta_{off} + \theta_{ov} \le \theta_p \le \theta_e) \end{cases} \tag{5}$$

where θ_{on}, θ_{off}, θ_{ov}, and T_e^* are turn-on angle, turn-off angle, over lapping angle, and the total torque reference. $\theta_e = 2\pi/N_r$ is the period of electrical angle.

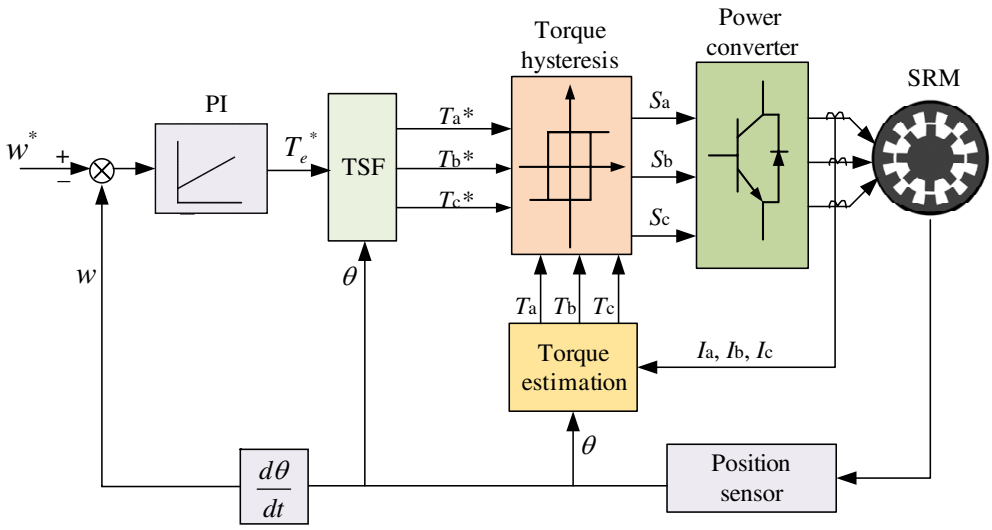

Figure 3. Control diagram of TSF-DITC method.

The power converter adopts an asymmetric half-bridge type converter, and each phase bridge arm is composed of 2 IGBTs. It is defined that the upper and lower arm IGBTs of the power converter are closed at the same time as $S = 1$; the upper arm IGBT is disconnected; the lower arm IGBT is closed as $S = 0$, and the upper and lower arm IGBTs are simultaneously disconnected as $S = -1$. Therefore, there are 3 switching states for each phase power converter, as shown in Figure 4.

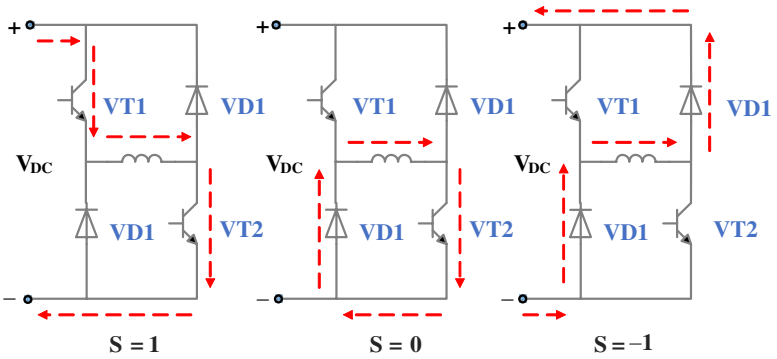

Figure 4. Asymmetric half bridge circuit.

3.2. Analysis of Torque Ripple

Although the traditional TSF-DITC control can reduce the torque ripple to a certain extent, the suppression effect is not complete, and the torque ripple in the commutation region is still relatively large. The reasons are as follows:

I. At the beginning of commutation of the motor, since the change rate of inductance in the motor model is relatively low, the actual torque generated by phase k (current phase) winding is small, which cannot track the theoretical torque value of this phase, resulting in the pulsation of the total torque.

II. Before the end of the commutation stage of the motor, due to the large change rate of inductance in the motor model at this time, the actual torque generated by the winding of phase $k-1$ (the previous phase) is large, which exceeds the theoretical torque value of this phase, resulting in the pulsation of the total torque.

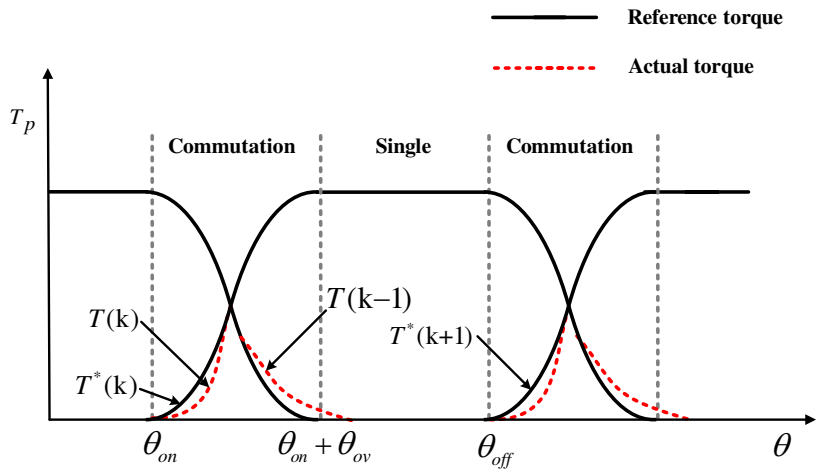

Figure 5. Comparison of phase reference torque and actual torque.

Figure 5 is a schematic diagram of the instantaneous output torque and its reference torque in the DITC based on the cosine TSF. In Figure 5, $T(k-1)$ represents the actual torque of the previous phase; $T(k)$, $T^*(k)$ represent the actual torque and reference torque of the current phase, respectively; and $T^*(k+1)$ is the reference torque of the next phase.

Therefore, in order to further suppress the torque ripple in the commutation region and consider the shortcomings of hysteresis control, a torque compensation method of switched reluctance motor using MPC based on TSF-DITC is proposed.

4. PRINCIPLE OF TSF-PDITC METHOD

The control diagram of this method is shown in Figure 6. First, the speed PI controller outputs the total reference torque value T_e^*, and the cosine TSF distributes the total reference torque value to individual phase reference torque value. Secondly, the prediction model calculates the torque value of the next sampling period, and to achieve optimal compensation of torque, the toque compensation module divides different sectors according to the rotor position to select different voltage states. Finally, a minimization performance cost function is designed, and the minimum predicted value is selected as the optimal voltage to control the motor at the next sampling time.

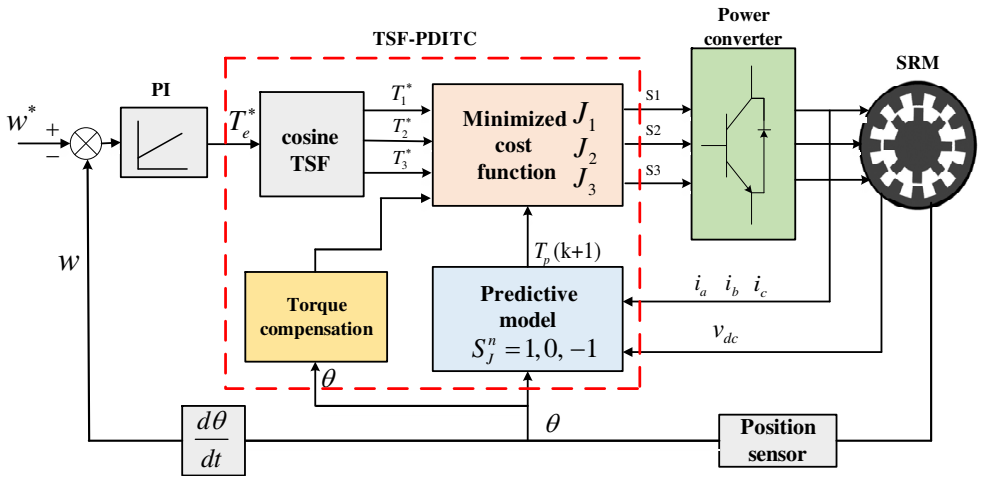

Figure 6. Control diagram of TSF-PDITC method.

4.1. Predictive Model and Cost Function

The derivative of phase current value can be obtained from (1), and the expression is as follows:

$$\frac{di_p}{dt} = \left(\frac{\partial \psi_p}{\partial i_p}\right)^{-1}\left[v_p - Ri_p - \frac{\partial \psi_p}{\partial \theta_p}\omega\right] \tag{6}$$

According to Equations (1), (3), (4), and (6), the discrete prediction model of the SRM can be obtained, as shown in the following Equation (7).

$$\begin{cases} \theta_p(k+1) = \theta_p(k) + \omega(k)T_s \\ i_p(k+1) = i_p(k) + T_s\left(\dfrac{\partial \psi_p(k)}{\partial i_p(k)}\right)^{-1}\left[v_p(k) - Ri_p(k) - \dfrac{\partial \psi_p(k)}{\partial \theta_p(k)}\omega(k)\right] \\ T_p(k+1) = \left[\dfrac{(L_{dsat} - L_q)i_p^2(k+1)}{2} + Ai_p(k+1) - \dfrac{A(1-e^{-Bi_p(k+1)})}{B}\right]\dfrac{df(\theta_p(k+1))}{dt} \\ T_e(k+1) = \sum_{p=1}^{3} T_p(k+1) \end{cases} \tag{7}$$

According to the above prediction model, the torque at the next moment can be predicted. The main goal of this paper is to achieve accurate tracking at a given torque value to minimize torque ripple. Therefore, the cost function (8) containing only one variable of torque is selected in this system.

$$J_p = \left|T_p^* - T_p(k+1)\right| \tag{8}$$

The advantage of this is that it can avoid the heavy trial and error work of weighting factors when there are multiple variables, and at the same time reduce the control complexity and calculation amount of the system.

4.2. Torque Compensation Scheme

In order to compensate for the torque tracking error in the commutation region and control the motor more accurately, different switch states are selected to control the motor in different position regions. According to the rotor position, this paper divides a working cycle into 9 sectors, which are divided into single-phase conduction region and commutation region. The commutation region is separated from $\theta_{on} + \theta_{ov}/2$ and divided into the first half of commutation and the second half of commutation. As shown in Figure 7, sectors I, IV, and VII are the first half of phase C $\rightarrow$ A, phase A $\rightarrow$ B, and phase B $\rightarrow$ C commutation, and sectors II, V, and VIII are the second half of phase C $\rightarrow$ A, phase A $\rightarrow$ B, and phase B $\rightarrow$ C commutation, respectively. Sectors III, VI, and IX are the single-phase conduction regions of phases A, B, and C, respectively.

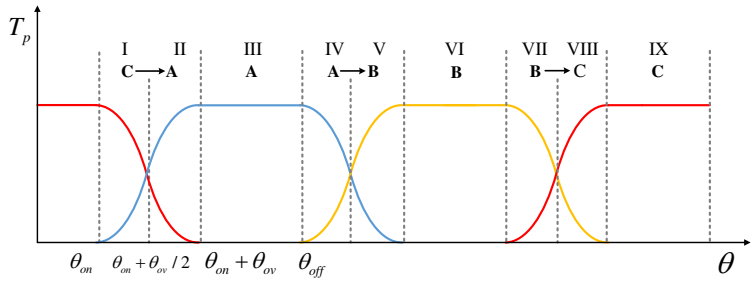

Figure 7. Sector partition of 12/8 SRM.

There are three candidate voltage states of 1, 0, and -1 in the single conduction phase interval, and the remaining two phases are -1.

In the commutation region, it is further divided into the first half of the commutation and the second half of the commutation.

I. In the first half of the commutation, the candidate voltage states of the excitation phase are 1 and 0, and the −1 is removed to make up for the impact of insufficient torque caused by the low inductance change rate; combined with the rules of the cosine TSF, the demagnetization phase is set to 1 and −1, ignores the 0, and keeps the 1 state in order to prevent the demagnetization phase torque from decreasing too fast, which will bring unnecessary torque ripple.

II. In the second half of the commutation, the demagnetization phase selects 0 and −1, and deletes the 1 state to avoid the influence of the actual torque being greater than the reference torque caused by the large inductance change rate; the excitation phase still retains 1 and 0 to ensure continuous and stable supply of excitation phase torque. The candidate voltage states corresponding to different sectors as depicted in Table 1.

Table 1. Candidate voltage states of each sector.

		Candidate voltage states		
	Sector	A	B	C
(C → A)	I	(1, 0)	−1	(1, −1)
	II	(1, 0)	−1	(0, −1)
(A)	III	(1, 0, −1)	−1	−1
(A → B)	IV	(1, −1)	(1, 0)	−1
	V	(0, −1)	(1, 0)	−1
(B)	VI	−1	(1, 0, −1)	−1
(B → C)	VII	−1	(1, −1)	(1, 0)
	VIII	−1	(0, −1)	(1, 0)
(C)	IX	−1	−1	(1, 0, −1)

For each phase of the 12/8 SRM, three possible voltage states need to be calculated in each sampling period, and the three-phase SRM needs to be calculated 9 times. After the sector is divided, the calculation amount is reduced from the original 9 times to 5 times, whether it is a single-phase conduction region or a commutation region. While reducing the amount of calculation, the control of SRM is also more precise. In summary, the specific implementation process of the TSF-PDITC algorithm is shown in Figure 8.

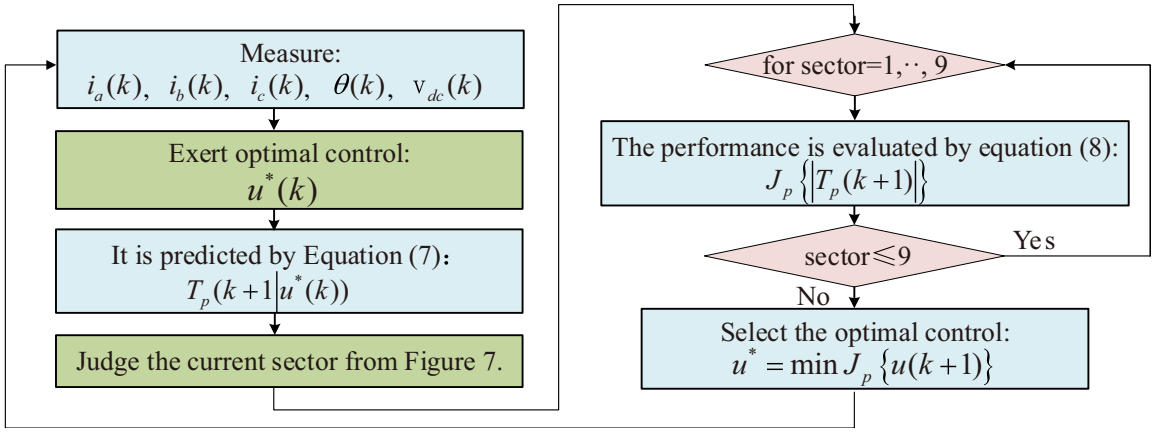

Figure 8. SRM TSF-PDITC flow chart.

5. SIMULATION RESULTS

In this paper, a simulation model is established with the parameters of a 2.2 kW three-phase 12/8-pole SRM. In the simulation, the proposed algorithm is compared with the TSF-DITC method. The sampling frequency is set to 100 kHz, the torque hysteresis width of the TSF-DITC algorithm set to ± 0.1, and the specific parameter of the selected motor is shown in Table 2.

Table 2. Parameters of the SRM.

Motor parameters	value	Motor parameters	value
Stator/rotor poles	12/8	Rated speed (r/min)	1500
Power (kW)	2.2	Stator resistance (Ω)	1.7
Rated torque ($N \cdot m$)	14	Moment of inertia ($kg \cdot m^2$)	0.01
L_q (H)	0.0308	L_d (H)	0.2154
L_{dsat} (H)	0.0199	Rated current (A)	12

5.1. Comparison before and after Torque Compensation in the Commutation Region

In Figure 9, the simulation results of reference torque and actual torque of two methods under 500 r/min and 5 $N \cdot m$ load torque are shown. According to Figure 9(a), it can be seen that the deviation between the reference torque curve and the actual torque curve before compensation is large. The reasons are detailed in Section 3.2. As can be seen from Figure 9(b), the reference torque curve after compensation basically coincides with the actual torque curve. This is because the method TSF-PDITC proposed in this paper divides sectors at the beginning and end of commutation, selects appropriate switching states to control the motor according to different sectors, compensates for the error between the actual output torque and the reference torque, and greatly reduces the total torque ripple.

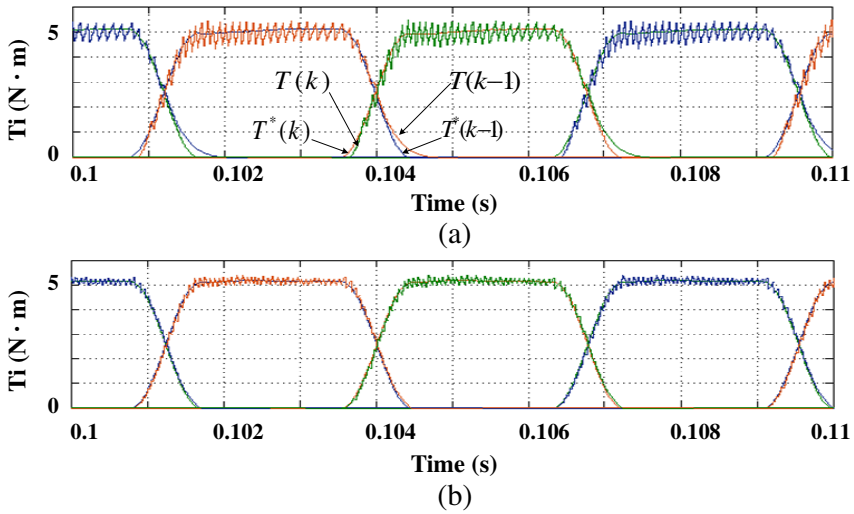

Figure 9. Simulation results of phase reference torque and actual torque at 500 r/min with 5 $N \cdot m$ load torque: (a) TSF-DITC; (b) TSF-PDITC.

5.2. Steady Performance

This paper uses T_{ripple} and T_{peak} as evaluation indicators to compare the two methods of TSF-DITC and TSF-PDITC, and define T_{ripple} and T_{peak} as the following formulas (9) and (10):

$$T_{ripple} = \frac{T_{\max} - T_{\min}}{T_{av}} \times 100\% \tag{9}$$

$$T_{peak} = T_{\max} - T_{\min} \tag{10}$$

Among them, T_{ripple} is the torque ripple coefficient; $T_{\max}$, $T_{\min}$, and T_{av} are the maximum torque value, minimum torque value, and average torque value, respectively; and T_{peak} is the peak-to-peak value of torque ripple.

When the speed is 200 r/min and the load torque 5 N · m, the traditional TSF-DITC simulation results are shown in Figure 10(a). Phase current i_p, phase torque T_i, and total torque T_e are presented in each subplot. It can be seen that the traditional TSF-DITC has obvious torque ripple, which is mainly caused by the tracking error between the actual torque and the reference torque during commutation.

However, as shown in Figure 10(b), TSF-PDITC has a better performance than TSF-DITC in reducing torque ripple. This shows that by embedding the cost function of MPC into the system instead of the torque hysteresis and selecting different switching states to control the motor relying on the sectors, the torque in the commutation region is effectively compensated, and the torque pulsation is greatly reduced.

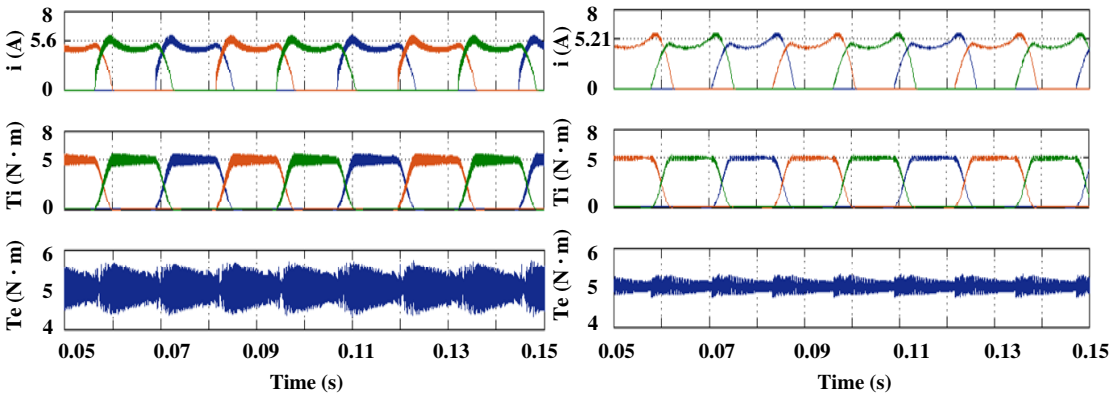

Figure 10. Simulation results of steady state at 200 r/min with 5 N · m load torque: (a) TSF-DITC; (b) TSF-PDITC.

In order to further evaluate the performance of the proposed algorithm, when the load torque is 5 N · m, the T_{peak} and T_{ripple} of the two methods at different speeds are calculated. As shown in Table 3, the T_{ripple} of TSF-PDITC is maintained at about 12%, while the T_{ripple} of TSF-DITC is greater than 25%.

Table 3. Comparison of T_{peak} and T_{ripple} at different speeds.

Method	TSF-DITC				TSF-PDITC			
Speed (r/min)	200	400	600	800	200	400	600	800
T_{peak} (N · m)	1.38	1.3	1.4	1.43	0.56	0.59	0.58	0.61
T_{ripple} (%)	26.98	25.7	27.37	27.66	12.39	11.47	11.34	11.74

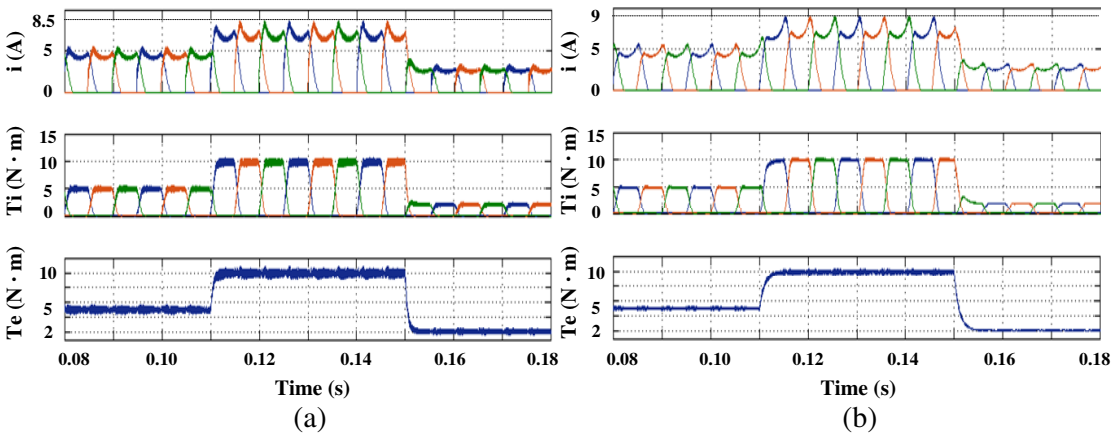

Figure 11. Simulation results of transient state at 500 r/min and load torque changed from 5–10 to 2 N · m: (a) TSF-DITC; (b) TSF-PDITC.

5.3. Transient Performance

The simulation conditions are as follows: the given speed of the motor is set to 500 r/min, and the load torque suddenly increases from 5 N · m to 10 N · m at 0.11 s and drops to 2 N · m at 0.15 s. Before and after increasing or decreasing the load torque, the torque ripple of the TSF-PDITC method is always kept at a lower level than that of the TSF-DITC, as shown in Figure 11.

After the load torque is increased from 5 to 10 N · m, the peak current of TSF-DITC is 8.52 A, and the peak current of TSF-PDITC is 7.99 A. Overall, the simulation results show that the TSF-PDITC control method has lower torque ripple and higher efficiency than TSF-DITC in the case of sudden load changes.

6. CONCLUSION

In this paper, a TSF-PDITC approach is proposed to reduce the torque pulsation of the conventional TSF-DITC. On the one hand, the MPC is integrated into the conventional TSF-DITC instead of hysteresis control, which effectively solves the problem of unfixed switching frequency. On the other hand, a scheme of torque compensation in the commutation region is proposed, which not only reduces the torque tracking error in the commutation region and further reduces the torque pulsation, but also reduces the number of candidate switching states and the computational effort. Also, by subdividing the rotor position into sectors, a more accurate control of SRM torque is achieved. Finally, the simulation results confirm that the TSF-PDITC method not only reduces the torque pulsation, but also has higher efficiency compared with the conventional TSF-DITC method.

REFERENCES

1. Bilgin, B., B. Howey, A. D. Callegaro, et al., "Making the case for switched reluctance motors for propulsion applications," *IEEE Transactions on Vehicular Technology*, Vol. 69, No. 7, 7172–7186, 2020.
2. Zan, X., Z. Jiang, K. Ni, et al., "Modular battery management for SRM drives in hybrid vehicles based on a novel modular converter," *IEEE AAccess*, Vol. 8, No. 1, 136296–136306, 2020.
3. Aiso, K. and A. Kan, "High speed SRM using vector control for electric vehicle," *Transactions on Electrical Machines and Systems*, Vol. 4, No. 1, 61–68, 2020.
4. Sun, Q., J. Wu, C. Gan, et al., "Multi-level converter-based torque sharing function control strategy for switched reluctance motors," *International Conference on Electrical Machines Systems*, 1–5, IEEE, 2017.

5. Liu, Y., L. I. Jie, and C. Shan, "Direct instantaneous torque control of switched reluctance motor based on optimal angle adaptive TSF," *Journal of Beijing University of Aeronautics and Astronautics*, Vol. 45, No. 11, 2152–2159, 2019.
6. Li, Z. and Z. Kan, "A high efficiency direct instantaneous torque control of SRM. Transactions of China Electro technical Society," *Transactions of China Electro technical Society*, Vol. 25, No. 8, 31–37, 2010.
7. Valenciagarcia, D. F., R. Tarvirdilu-Asl, C. Garcia, et al., "A review of predictive control techniques for switched reluctance machine drives," *IEEE Transactions on Energy Conversion*, Vol. 36, No. 2, 1323–1335, 2020.
8. Valenciagarcia, D. F., R. Tarvirdilu-Asl, C. Garcia, et al., "A review of predictive control techniques for switched reluctance machine drives. Part II: Torque control, assessment and challenges," *IEEE Transactions on Energy Conversion*, Vol. 36, No. 2, 1323–1335, 2020.
9. Elmorshedy, M. F., W. Xu, F. El-Sousy, et al., "Recent achievements in model predictive control techniques for industrial motor: A comprehensive state-of-the-art," *IEEE Access*, Vol. 9, No. 1, 58170–58191, 2021.
10. Shang, C., A. Xu, L. Huang, et al., "Flux linkage optimization for direct torque control of switched reluctance motor based on model predictive control," *IEEE Transactions on Electrical and Electronic Engineering*, Vol. 14, No. 7, 1105–1113, 2019.
11. Hu, K., L. Guo, and J. Ye, "Model predictive current control of mutually coupled switched reluctance machines using a three-phase voltage source converter," *IEEE Applied Power Electronics Conference and Exposition (APEC)*, 704–710, New Orleans, 2020.
12. Le-Huy, H. and P. Brunelle, "A versatile nonlinear switched reluctance motor model in Simulink using realistic and analytical magnetization characteristics," *Industrial Electronics Society*, 6, 2005.